European Journal of Medicinal Chemistry 46 (2011) 3282–3290

Contents lists available at ScienceDirect

European Journal of Medicinal Chemistry

journal homepage: http://www.elsevier.com/locate/ejmech

Original article

Synthesis, cellular uptake, apopotosis, cytotoxicity, cell cycle arrest, interaction with DNA and antioxidant activity of ruthenium(II) complexes

Hong-Liang Huang [a], Zheng-Zheng Li [b], Zhen-Hua Liang [b], Jun-Hua Yao [c], Yun-Jun Liu [b,d,*]

[a] School of Life Science and Biopharmaceutical, Guangdong Pharmaceutical University, Guangzhou 510006, PR China
[b] School of Pharmacy, Guangdong Pharmaceutical University, Guangzhou 510006, PR China
[c] Instrumentation Analysis and Research Center, Sun Yat-Sen University, Guangzhou 510275, PR China
[d] School of Chemistry and Chemical Engineering, Guangdong Pharmaceutical University, Guangzhou 510006, PR China

ARTICLE INFO

Article history:
Received 9 February 2011
Received in revised form
15 April 2011
Accepted 19 April 2011
Available online 29 April 2011

Keywords:
Ruthenium(II) complexes
Cytotoxicity
Apoptosis
Cellular uptake
DNA-binding

ABSTRACT

A new ligand and two ruthenium(II) complexes $[Ru(bpy)_2(DNPIP)](ClO_4)_2$ **1** and $[Ru(bpy)_2(DAPIP)](ClO_4)_2$ **2** were synthesized and characterized. The DNA-binding constants for complexes **1** and **2** were determined to be 2.24 (±0.30) × 10^5 M^{-1} ($s = 1.29$) and 6.34 (±0.32) × 10^4 M^{-1} ($s = 2.84$). The photocleavage of pBR322 DNA by Ru(II) complexes was investigated. The cytotoxicity of complexes **1** and **2** were assessed against three tumor cell lines. The apoptosis and cellular uptake were studied. The retardation assay of pGL 3 plasmid DNA was explored. The cell cycle arrest was analysized by flow cytometry. The antioxidant activities of the ligand and complexes were also investigated.

1. Introduction

Cisplatin (cis-diamminedichloroplatinum) and its analogs are a class of widely used antitumor drug. The antitumor activity of them derives from its binding to DNA and formation of covalent cross-links [1–4]. Due to significant side effect, including nephrotoxicity, gastrointestinal toxicity, neurotoxicity, and totoxicity, low water solubility, and drug resistance have limited the clinical applications of cisplatin. These limitations of cisplatin have motivated extensive investigations into alternative metal-based cancer therapies. Ruthenium complexes, as the substituents of cisplatin, possess several favorable properties suited to rational anticancer drug design and biological applications. A number of ruthenium complexes have been shown to display high anticancer activities. NAMI-A and KP109 have entered clinical trials [5,6]. Complex $[Ru(bpy)_2(dppn)]^{2+}$ exhibits high cytotoxicity against human MCF-7 cancer cell lines comparable to that of cisplatin [7]. $[Ru(phen)_2(p\text{-}MOPIP)]^{2+}$ can effectively inhibit the proliferation of HepG-2 cell line with low IC_{50} value (7.2 ± 1.3 μM) [8], and $[Ru(phen)_2(DBHIP)]^{2+}$ can effectively induce apoptosis of BEL-7402 cell line [9]. In this report, we report the synthesis, characterization of a new ligand DNPIP and two ruthenium(II) polypyridyl complexes: $[Ru(bpy)_2(DNPIP)]^{2+}$ **1** (bpy = 2,2′-bipyridine, DNPIP = 2-(2,4-dinitrophenyl)imidazo [4,5-*f*][1,10]phenanthroline) and $[Ru(bpy)_2(DAPIP)]^{2+}$ **2** (DAPIP = 2-(2,4-diaminophenyl)imidazo [4,5-*f*][1,10] phenanthroline, Scheme 1). Their DNA-binding behaviors were studied by electronic absorption titration, viscosity measurements, thermal denaturation, and photoactivated cleavage. The results indicated that complexes **1** and **2** can intercalate between the base pairs of DNA. The cytotoxicity of complexes **1** and **2** has been evaluated by MTT (MTT = (3-(4,5-dimethylthiazol-2-yl)-2,5-diphenyltetrazolium bromide)) assay. The apoptosis of BEL-7402 cells induced by Ru(II) complexes was also studied. The cellular uptake with Human hepatocellular carcinoma cell line (BEL-7402) was carried out and the results were observed under fluorescence microscopy. The cell cycle arrest was analyzed by flow cytometry.

Abbreviations: DNPIP, 2-(2,4-dinitrophenyl)imidazo[4,5-*f*][1,10]phenanthroline; DAPIP, 2-(2,4-diaminophenyl)imidazo[4,5-*f*][1,10]phenanthroline; Bpy, 2,2′-bipyridine; MTT, 3-(4,5-dimethylthiazol-2-yl)-2,5-diphenyltetrazolium bromide; AO, acridine orange; EB, ethidium bromide; DMSO, dimethyl sulfoxide; RPMI, Roswell Park Memorial Institute; DMF, N,N-dimethylformamide; CT-DNA, calf thymus DNA; MLCT, metal to ligand charge transfer; Tris, tris(hydroxymethyl)aminomethane; ES-MS, electrospray mass spectroscopy.

* Corresponding author. School of Pharmacy, Guangdong Pharmaceutical University, Guangzhou 510006, PR China. Tel.: +86 20 39352122; fax: +86 20 39352128.
E-mail address: lyjche@163.com (Y.-J. Liu).

0223-5234/$ – see front matter
doi:10.1016/j.ejmech.2011.04.049

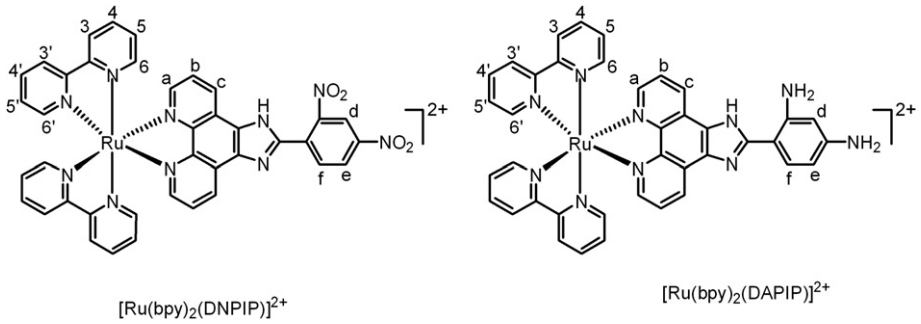

Scheme 1. The structure of complexes.

The antioxidant activity of the ligand and relative complexes was explored by hydroxyl radical (•OH) scavenging method in vitro.

2. Results and discussion

2.1. Electronic absorption titration

Absorption spectra titrations were performed to determine the DNA-binding affinity of complexes **1** and **2**. DNA sample was added in aliquots sequentially to complex solutions, with absorbance spectra recorded after each addition. The absorption spectra of complexes **1** and **2** in the absence and presence of CT-DNA are given in Fig. 1. As increasing concentration of DNA, the MLCT (metal-to-ligand charge transfer) transition bands of complexes **1** at 461 and **2** at 459 nm exhibit hypochromism of about 24.81 and 25.34%, and bathochromism of 2 and 3 nm, respectively. The DNA-binding affinity was derived by monitoring the change in absorbance of complexes **1** and **2** at the MLCT bands upon addition of CT DNA. The values of K for **1** and **2** are determined to be $2.24\ (\pm 0.30) \times 10^5\ M^{-1}$ ($s = 1.29$) and $6.34\ (\pm 0.32) \times 10^4\ M^{-1}$ ($s = 2.84$), respectively. These values are comparable to that of complexes $[Ru(bpy)_2(pip)]^{2+}$ ($4.70 \pm 0.20 \times 10^5\ M^{-1}$) [10], $[Ru(bpy)_2(m\text{-}npip)]^{2+}$ ($2.40 \pm 0.30 \times 10^5\ M^{-1}$) [11], but smaller than that of $[Ru(bpy)_2(HBT)]^{2+}$ ($5.71 \pm 0.20 \times 10^7\ M^{-1}$) [12].

2.2. Luminescence studies

Complexes **1** and **2** can luminesce in Tris buffer at room temperature with a maximum appearing at 599 and 600 nm, respectively. Fig. 2 showed the luminescence spectra of the complexes in the absence and presence of increasing concentration of DNA in buffer solution. The emission intensities of complexes **1** and **2** increase to 5.73 and 1.53 times of the original intensities, respectively. The enhancement of emission intensity is an indication of binding of the complexes to the hydrophobic pocket of DNA, and complexes can be protected efficiently by the hydrophobic environment inside the DNA helix.

2.3. Viscosity measurements

To investigate further the DNA-binding mode of complexes **1** and **2**, viscosity measurements on solutions of CT DNA incubated with the complexes were performed. It is popularly accepted that a partial and/or nonclassical intercalation of ligand could bend (or kink) the DNA helix, reduces its effective length and, concomitantly, its viscosity; A classical intercalation of a ligand into DNA is known to cause a significant increase in the viscosity of a DNA solution due to an increase in the separation of the base pairs at the intercalation site and, hence, an increase in the overall DNA molecular length [13]. When complexes **1** and **2** are treated with CT DNA (0.25 mM) and the concentrations of ruthenium complexes are increased from a ratio of $R = 0$–0.16 ($R = [Ru]/[DNA]$), the relative viscosity of DNA increases steadily (Fig. 3) in the order **1** > **2**. These results showed that complexes **1** and **2** interact with DNA through intercalative mode.

2.4. Thermal denaturation

The thermal denaturation was studied by monitoring the change in absorbance spectrum of the DNA solution ($\lambda = 260$ nm). The effect of complexes **1** and **2** on the melting temperature of CT DNA in buffer is shown in Fig. 4. In the absence of any added

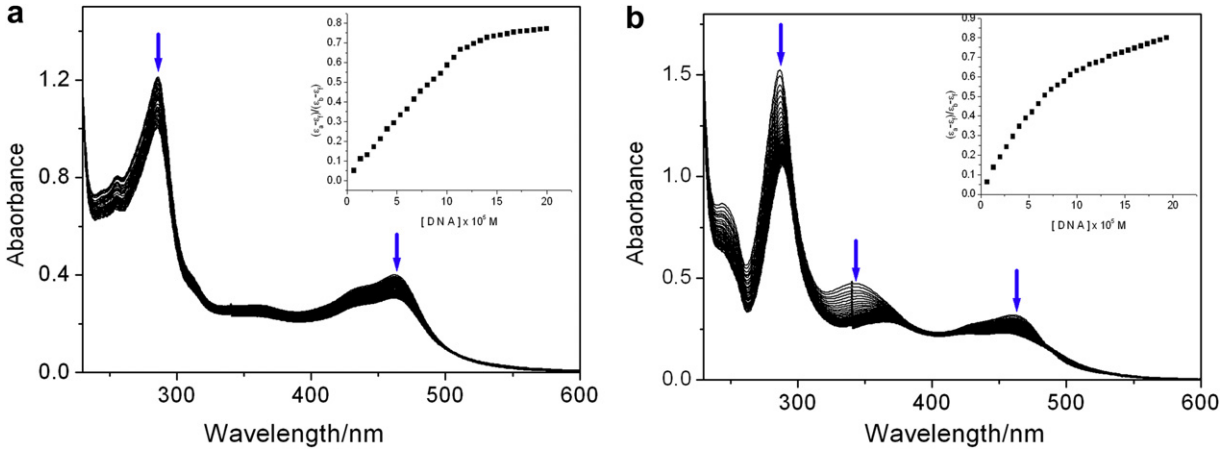

Fig. 1. Absorption spectra of complexes **1** (a) and **2** (b) in Tris–HCl buffer upon addition of CT-DNA. [Ru] = 20 μM. Arrow shows the absorbance change upon the increase of DNA concentration. Plots of $(\varepsilon_a - \varepsilon_f)/(\varepsilon_b - \varepsilon_f)$ versus [DNA] for the titration of DNA with Ru(II) complexes.

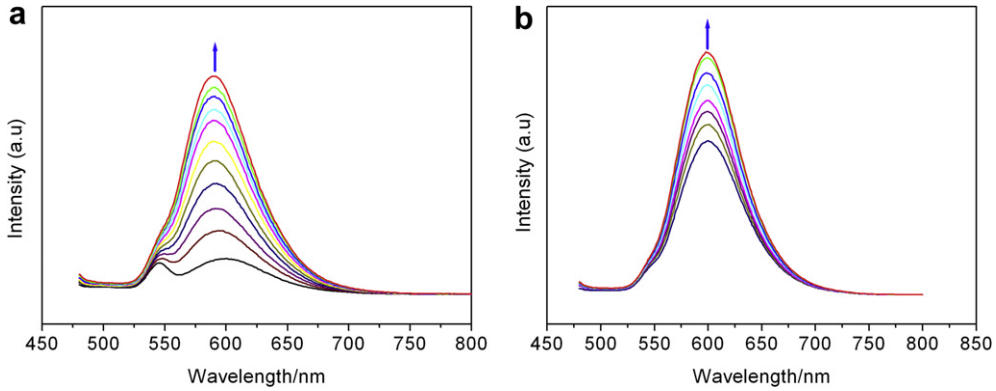

Fig. 2. Emission spectra of complexes (a) **1** and (b) **2** in Tris–HCl buffer in the absence and presence of CT-DNA. Arrow shows the intensity change upon increasing DNA concentrations.

complexes, the thermal denaturation carried out for DNA gave a T_m of 59.99 ± 0.3 °C under our experimental conditions. The observed melting temperature in the presence of complexes **1** and **2** were 67.99 ± 0.3 °C and 66.85 ± 0.3 °C, respectively. Thus, it could be rationally concluded that the complexes **1** and **2** are a typical DNA intercalator, and the π–π stacking between inserting ligand DNPIP or DAPIP and base pairs may effectively stabilize the DNA double helix configuration. The large increases in T_m of the two Ru(II) complexes (the ΔT_m is 8.00 and 6.86 °C) are comparable to those observed for Ru(II) complexes [14–17].

2.5. Gel electrophoresis shift assay

The cleavage reaction on plasmid DNA induced by ruthenium(II) complexes were performed and monitored by agarose gel electrophoresis. Fig. 5 showed gel electrophoresis separation of pBR322 DNA after incubation with different concentrations of Ru(II) complexes and irradiation at 365 nm for 30 min. No obvious DNA cleavage was observed for control in which complex was absent, or incubation of the plasmid with the Ru(II) complex in darkness. As increasing concentrations of complexes **1** and **2**, the amount of Form I (supercoiled form) of pBR 322 DNA diminishes gradually, whereas that of Form II (circular form) increases. These results indicate that scission occurs on one strand (nicked). Under the same experimental conditions, complex **2** exhibits more effective DNA cleavage activity than complex **1**. The different cleaving efficiency is not consistent with the DNA-binding affinity of two Ru(II) complexes.

2.6. Retardation of pGL 3 plasmid DNA

Retardation of pGL 3 DNA was carried out with saline (0.9%) as buffer solution. DNA condensation into contact structures has been received considerable attention to understand the mechanism of uptake of gene vectors in living cells. Fig. 6 showed that complexes **1** and **2** cannot condense the DNA when the concentrations of **1** and **2** are 1 and 2 mM. However, at the concentrations of 4 and 6 mM for complex **1** or 6 mM for complex **2**, the effects of condensation of DNA were obviously observed.

2.7. Cytotoxicity assay in vitro

The cytotoxicity in vitro assay for complexes was assessed using the method of MTT reduction. Cisplatin was used as a positive control. After treatment of BEL-7402, HepG-2 and MCF-7 cell lines for 48 h with complexes **1** and **2** in the range of concentration (6.25 → 400 μM). The inhibitory percentage against growth of cancer cells was determined. The cell viability (%) obtained with continuous exposure for 48 h are depicted in Fig. 7. The cytotoxicity of complexes was found to be concentration-dependent. The cell viability decreased with increasing the concentrations of complexes **1** and **2**. The IC_{50} were calculated and listed in Table 1. The IC_{50}

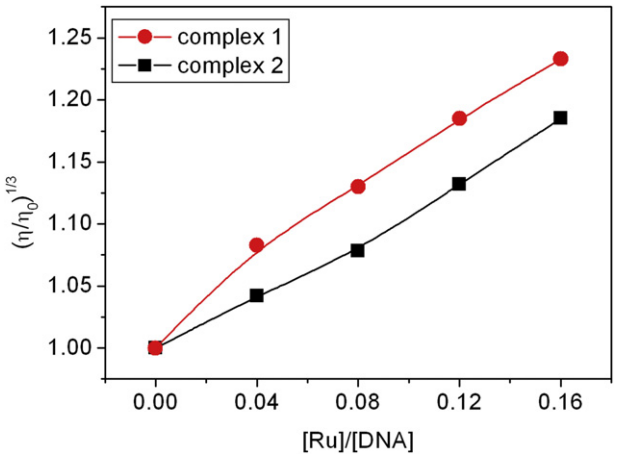

Fig. 3. Effect of increasing amounts of complexes **1** (●) and **2** (■) on the relative viscosity of calf thymus DNA at 25 (±0.1) °C. [DNA] = 0.25 mM.

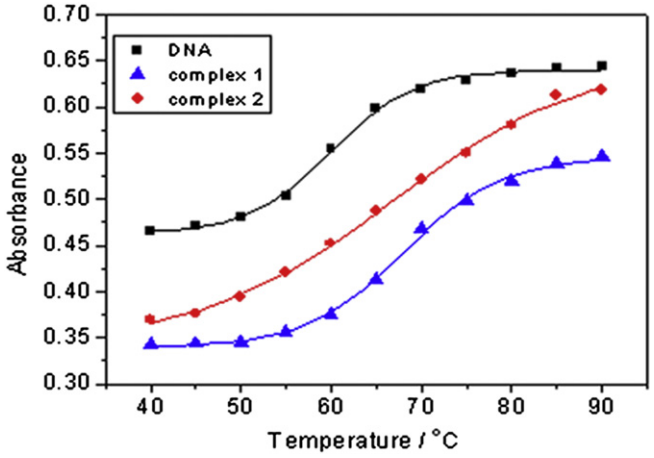

Fig. 4. Thermal denaturation of CT-DNA in the absence (■) and presence of complexes **1** (▲) and 2 (●). [Ru] = 30 μM, [DNA] = 80 μM.

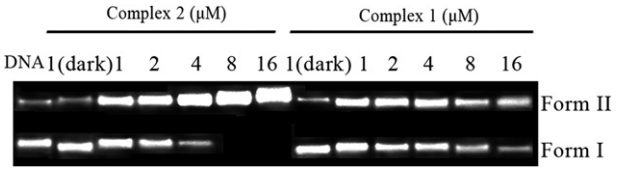

Fig. 5. Photoactivated cleavage of pBR 322 DNA in the presence of different concentrations of Ru(II) complexes after irradiation at 365 nm for 30 min.

values are 45.75, 97.84 and 68.80 for complex **1**, 105.48, 52.87 and 77.98 for complex **2**, respectively. Comparing the IC_{50} values of complexes **1** and **2**, complex **2** appeared to be more active against HepG-2 and MCF-7 cell lines than complex **1**. This is not consistent with the DNA-binding affinities of complexes **1** and **2**. Furthermore, these complexes are lower in cytotoxicity than those of cisplatin under the identical condition.

2.8. Apoptosis activity

Most of the cytotoxic drugs in current use have been shown to induce apoptosis in susceptible cells. The fact that disparate agents, which interact with different targets, induce cell death with some common features (endonucleolytic cleavage of DNA, changes in chromatin condensation) suggests that cytotoxicity is determined by the ability of the cell to engage this so-called "programmed" cell death [18]. To further address the death pattern, BEL-7402 cells were stained with acridine orange (AO) and ethidium bromide (EB). The AO/EB staining is sensitive to DNA and was used to access changes in nuclear morphology. In the absence of complex **2**, the living cells were stained bright green in spots (Fig. 8A). After treatment of BEL-7402 cells with complex **2** for 48 h, the green apoptotic cells with apoptotic features such as nuclear shrinkage, chromatin condensation, as well as red necrotic cells, were observed (Fig. 8B). Similar results for complex **1** were also observed.

2.9. Flow cytometric analysis

The effect of complex **1** on cell cycle of BEL-7402 and HepG-2 cells was investigated by flow cytometry in PI (propidium iodide) stained cells after Ru(II) complex treatment for 24 h. Fig. 9 showed the representative DNA distribution histograms of BEL-7402 and HepG-2 cells in the absence (A for BEL-7402 and C for HepG-2) and presence of complex **1** (B for BEL-7402 and D for HepG-2). Fig. 9 showed that the treatment of BEL-7402 cells with complex **1** caused a obvious increase in the percentage of cells at G2/M phase, accompanied by corresponding reduction in the percentage of cells in G0/G1 phase, indicating the induction of G2/M phase arrest by complex **1**. While treatment of HepG-2 with complex **1**, a large increase (16.27%) in the percentage of cells at S phase and corresponding reduction at G0/G1 phase were observed, and a concomitant increase in the population of Sub-G1 phase cells were also observed, which suggested the antiproliferative mechanism on HepG-2 was S phase arrest. These results showed complex **1** exhibited different antiproliferative mechanism against different cancer cells.

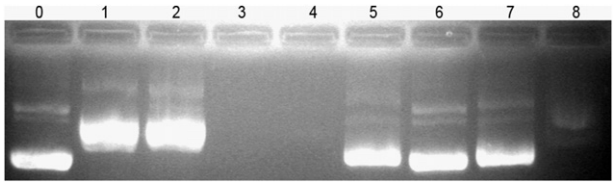

Fig. 6. Agarose gel electrophoresis retardation of pGL 3 plasmid DNA in the presence different concentrations of complexes **1** and **2**. Lane 0 (DNA alone); 2: (1) 1 mM; (2) 2 mM; (3) 4 mM; (4) 6 mM. 1: (5) 1 mM; (6) 2 mM; (7) 4 mM; (8) 6 mM [DNA] = 0.5 μg.

2.10. Cellular uptake

In the functional study, the cellular uptake of complex **2** (50 μM) by BEL-7402 cells was studied using fluorescence microscopy. After treatment of BEL-7402 cells with complex **2** for 48 h and removing the culture medium, the cells were observed under fluorescent microscopy. As shown in Fig. 10, the bright red fluorescent spots in the images were observed indicated that the complex **2** can enter into the cytoplasm and accumulate in the nuclei, however, no any red fluorescent spot was observed in the control (data not presented). These results showed that the cellular uptake was successfully observed. Similar results for complex **1** were also observed.

2.11. Antioxidant activity against hydroxyl radical (˙OH)

Oxidative damage to DNA has been suggested to contribute to aging and various diseases including cancer and chronic inflammation [19]. Among all reactive oxygen species, the hydroxyl radical (˙OH) is by far the most potent and therefore the most dangerous oxygen metabolite, elimination of this radical is one of the major aims of antioxidant administration [20]. The hydroxyl radical (˙OH) in aqueous media was generated by the Fenton system. The antioxidant activity of complexes **1** and **2** together with ligand DNPIP was investigated. The inhibitory effect was depicted in Fig. 11, and the suppression ratio was listed in Table 2. The average suppression ratio valued from 3.08 to 31.61% for DNPIP, 0.51 to 45.24% for complex **1**, 1.08 to 48.33% for complex **2**. The antioxidant activity against hydroxyl radical of complexes **1** and **2** is comparable under the same experimental condition. It is clear that complexes **1** and **2** have high antioxidant activity and we can conclude that the hydroxyl radical scavenging ability can be enhanced when ligand bonds metal center to form complexes. Similar results were observed for other ruthenium(II) complexes [21]. The information obtained from the present work would be helpful to develop new potential antioxidants and some new therapeutic reagents for some diseases.

3. Conclusion

Two new ruthenium(II) polypyridyl complexes $[Ru(bpy)_2(DNPIP)]^{2+}$ **1** and $[Ru(bpy)_2(DAPIP)]^{2+}$ **2** were synthesized and characterization. The DNA-binding behaviors show that the two complexes interact with CT DNA through intercalative mode. The cytotoxicity assay indicates that complexes **1** and **2** can inhibit the proliferation. The apoptotic study exhibits that complexes **1** and **2** can effectively induce the apoptosis of BEL-7402 cells. The flow cytometric analysis shows that treatment of BEL-7402 and HepG-2 cells with complex **1** indicates the induction of G2/M and S phase arrest, respectively. And the cellular uptake suggests that these complexes can enter into the cytoplasm and accumulate in the nuclei. Antioxidant activity shows that the two complexes may be potential drugs to eliminate the hydroxyl radical.

4. Experimental

4.1. Materials and methods

Calf thymus DNA (CT-DNA) was obtained from the Sino-American Biotechnology Company. pBR 322 DNA was obtained from Shanghai Sangon Biological Engineering & Services Co., Ltd. Dimethyl sulfoxide (DMSO) and RPMI 1640 were purchased from Sigma. Cell lines of

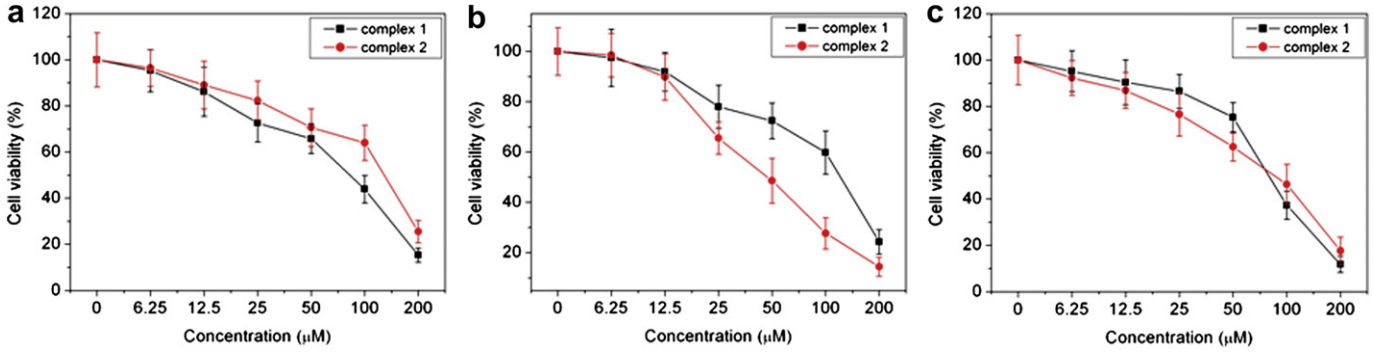

Fig. 7. Cell viability of complexes **1** and **2** on tumor BEL-7402 (a), HepG-2 (b) and MCF-7 (c) cell proliferation in vitro. Each data point is the mean ± standard error obtained from at least three independent experiments.

BEL-7402 (hepatocellular), HepG-2 (hepatocellular) and MCF-7 (breast cancer) were purchased from American Type Culture Collection, agarose and ethidium bromide were obtained from Aldrich. $RuCl_3 \cdot xH_2O$ was purchased from Kunming Institution of Precious Metals. 1,10-phenanthroline was obtained from Guangzhou Chemical Reagent Factory. Doubly distilled water was used to prepare buffers (5 mM Tris(hydroxymethylaminomethane)-HCl, 50 mM NaCl, pH = 7.2). A solution of calf thymus DNA in the buffer gave a ratio of UV absorbance at 260 and 280 nm of ca. 1.8–1.9:1, indicating that the DNA was sufficiently free of protein [22]. The DNA concentration per nucleotide was determined by absorption spectroscopy using the molar absorption coefficient (6600 M^{-1} cm^{-1}) at 260 nm [23].

Microanalysis (C, H, and N) was carried out with a Perkin–Elmer 240Q elemental analyzer. Fast atom bombardment (FAB) mass spectra were recorded on a VG ZAB-HS spectrometer in a 3-nitrobenzyl alcohol matrix. Electrospray mass spectra (ES-MS) were recorded on a LCQ system (Finnigan MAT, USA) using methanol as mobile phase. The spray voltage, tube lens offset, capillary voltage and capillary temperature were set at 4.50 KV, 30.00 V, 23.00 V and 200 °C, respectively, and the quoted *m/z* values are for the major peaks in the isotope distribution. ^{1}H NMR spectra were recorded on a Varian-500 spectrometer. All chemical shifts were given relative to tetramethylsilane (TMS). UV/Vis spectra were recorded on a Shimadzu UV-3101PC spectrophotometer at room temperature.

4.2. Synthesis of ligand and complexes

4.2.1. Synthesis of ligand (DNPIP)

A mixture of 1,10-phenanthroline-5,6-dione (0.315 g, 1.5 mmol) [24], 2,4-dinitrobenzaldehyde (0.294 g, 1.5 mmol), ammonium acetate (2.31 g, 30 mmol) and glacial acetic acid (20 cm^3) was refluxed with stirring for 2 h. The cooled solution was diluted with water and neutralized with concentrated aqueous ammonia. The precipitate was collected and purified by column chromatography on silica gel (60–100 mesh) with ethanol as eluent to give the compound as yellow powder. Yield: 80%. Anal. Calcd. for $C_{19}H_{10}N_6O_4$: C, 59.07; H, 2.61; N, 21.75; Found: C, 59.01; H, 2.54; N, 21.53%. ES-MS: $m/z = 387.2$ $[M + H]^+$. ^{1}H NMR (500 MHz, DMSO-d_6): 9.08 (d, 1H, J = 8.2 Hz), 8.91 (d, 2H, J = 8.0 Hz), 8.79 (d, 1H, J = 8.5 Hz), 8.75 (d, 1H, J = 8.0 Hz), 8.44 (d, 2H, J = 8.5 Hz), 7.87 (dd, 2H, J = 5.5 Hz, J = 5.0 Hz).

Table 1
The IC_{50} values of complexes **1** and **2** against the selected cell lines.

Compound	IC_{50}(μM)		
	BEL-7402	HepG-2	MCF-7
1	45.75 ± 3.04	97.82 ± 3.23	68.80 ± 3.15
2	105.48 ± 5.13	52.87 ± 3.56	77.98 ± 3.41
Cisplatin	19.78 ± 2.55	25.48 ± 3.15	12.24 ± 2.55

4.2.2. Synthesis of $[Ru(bpy)_2(DNPIP)](ClO_4)_2 \cdot 2H_2O$ (**1**)

A mixture of *cis*-$[Ru(bpy)_2Cl_2] \cdot 2H_2O$ (0.280 g, 0.5 mmol) [25] and DNPIP (0.193 g, 0.5 mmol) in ethylene glycol (20 cm^3) was refluxed under argon for 8 h to give a clear red solution. Upon cooling, a red precipitate was obtained by dropwise addition of saturated aqueous $NaClO_4$ solution. The crude product was purified by column chromatography on a neutral alumina with a mixture of CH_3CN-toluene (3:1, v/v) as eluent. The main red band was collected. The solvent was removed under reduced pressure and a red powder was obtained. Yield: 71%. Anal. Calcd. for $C_{39}H_{26}N_{10}Cl_2O_{12}Ru \cdot 2H_2O$: C, 45.46; H, 2.92; N, 13.54; Found: C, 45.27; H, 3.32; N, 13.48%. ES-MS [CH_3CN, *m/z*]: 799.2 ($[M-2ClO_4-H]^+$), 400.3 ($[M-2ClO_4]^{2+}$). ^{1}H NMR (500 MHz, DMSO-d_6): δ 9.08 (d, 1H, H_d, J = 7.8 Hz), 9.03 (d, 2H, H_c, J = 8.0 Hz), 8.87 (dd, 4H, $H_{3,3'}$, J = 8.0, J = 8.0 Hz), 8.67 (d, 2H, H_a, J = 8.4 Hz), 8.48 (d, 1H, H_e, J = 6.5 Hz), 8.24 (t, 2H, H_4, J = 7.6 Hz), 8.10 (t, 2H, $H_{4'}$, J = 7.5 Hz), 7.88 (d, 2H, H_6, J = 5.5 Hz), 7.82 (d, 2H, $H_{6'}$, J = 5.5 Hz), 7.74 (q, 1H, H_f), 7.60 (dd, 2H, H_b, J = 5.5, J = 6.0 Hz), 7.38 (t, 2H, H_5, J = 7.6 Hz), 7.23 (t, 1H, $H_{5'}$, J = 7.5 Hz), 7.17 (t, 1H, $H_{5'}$, J = 7.8 Hz).

4.2.3. Synthesis of $[Ru(bpy)_2(DAPIP)](ClO_4)_2 \cdot 1.5H_2O$ (**2**)

A mixture of $[Ru(bpy)_2(DNPIP)](ClO_4)_2 \cdot 2H_2O$ (0.541 g, 0.5 mmol) was completely dissolved in minimum amount of acetonitrile, Then the Pd/C (0.20 g, 10% Pd), $NH_2NH_2 \cdot H_2O$ (8 cm^3) and ethanol (20 cm^3) were added in the above solution and refluxed under argon for 8 h. The hot solution was filtered and evaporated under reduced pressure to remove the solvent to 6 cm^3. Upon cooling, a red precipitate was obtained by dropwise addition of saturated aqueous $NaClO_4$ solution. The crude product was purified by column chromatography on a neutral alumina with a mixture of CH_3CN-toluene (3:1, v/v) as eluent. The main red band was collected. The solvent was removed under reduced pressure and a red powder was obtained. Yield: 70%. Anal. Calcd. for $C_{39}H_{30}N_{10}Cl_2O_8Ru \cdot 1.5H_2O$: C, 48.50; H, 3.45; N, 14.51; Found: C, 48.88; H, 3.89; N, 14.37%. ES-MS [CH_3CN, *m/z*]: 887.00 ($[M-ClO_4]^+$), 738.4 ($[M-2ClO_4-H]^+$), 369.6 ($[M-2ClO_4]^{2+}$). ^{1}H NMR (500 MHz, DMSO-d_6): δ 9.12 (d, 2H, H_c, J = 8.5 Hz), 8.86 (dd, 4H, $H_{3,3'}$, J = 8.5, J = 8.0 Hz), 8.22 (d, 2H, H_a, J = 8.0 Hz), 8.10 (t, 2H, H_4, J = 7.5 Hz), 8.01(t, 2H, $H_{4'}$, J = 7.0 Hz), 7.84–7.92 (m, 4H, $H_{6,6'}$), 7.70 (d, 1H, H_f, J = 8.0 Hz), 7.59 (t, 4H, $H_{5,5'}$, J = 6.5 Hz), 7.34 (t, 2H, H_b, J = 6.5 Hz), 6.05 (t, 2H, $H_{d,e}$, J = 7.8 Hz), 5.47 (s, 4H, H_{NH_2}).

Caution: Perchlorate salts of metal compounds with organic ligands are potentially explosive, and only small amounts of the material should be prepared and handled with great care.

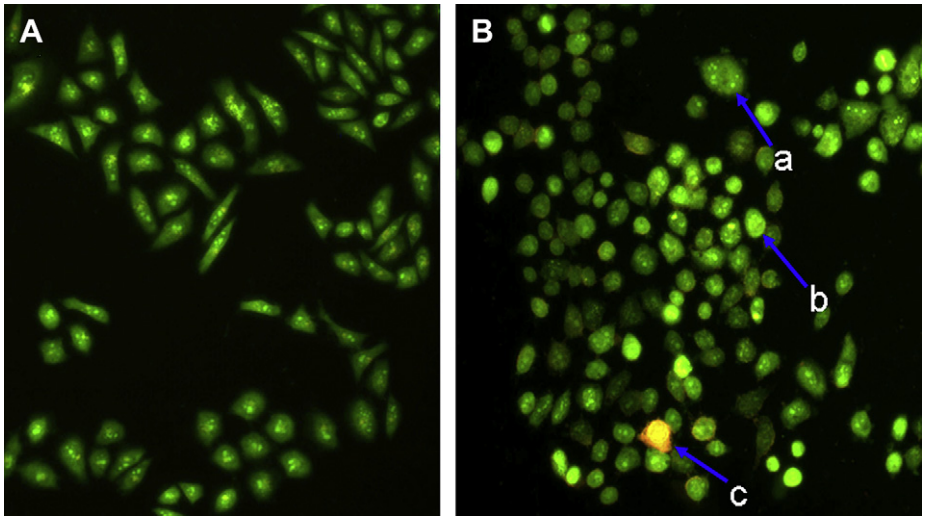

Fig. 8. BEL-7402 cell was stained by AO/EB and observed under fluorescence microscopy. BEL-7402 cell without treatment (A) and in the presence of complex 2 (B) incubated at 37 °C and 5% CO_2 for 48 h. Cells in a, b and c are living, apoptotic and necrotic cells, respectively.

4.3. DNA binding and photoactivated cleavage

The DNA-binding and photoactivated cleavage experiments were performed at room temperature. Buffer A [5 mM tris(hydroxymethyl)aminomethane (Tris) hydrochloride, 50 mM NaCl, pH 7.0] was used for absorption titration, luminescence titration and viscosity measurements. Buffer B (50 mM Tris–HCl, 18 mM NaCl, pH 7.2) was used for DNA photocleavage experiments. Buffer C (1.5 mM Na_2HPO_4, 0.5 mM NaH_2PO_4, 0.25 mM Na_2EDTA, pH 7.0) was used for thermal DNA denaturation experiments. Buffer D (0.9% of physiological saline) was used for retardation assay of pGL 3 plasmid DNA.

The absorption titrations of the complex in buffer were performed using a fixed concentration (20 μM) for complex to which increments of the DNA stock solution were added. Ru-DNA solutions were allowed to incubate for 5 min before the absorption spectra were recorded. The intrinsic binding constants K, based on the absorption titration, were measured by monitoring the changes of absorption in the MLCT band with increasing concentration of DNA using the following equation [26].

$$\left(\varepsilon_a-\varepsilon_f\right)\Big/\left(\varepsilon_b-\varepsilon_f\right)=b-\left(b^2-2K^2C_t[\mathrm{DNA}]/s\right)^{1/2}/2KC_t \qquad (1a)$$

$$(b\ =\ 1+KC_t+K[\mathrm{DNA}]/2s) \qquad (1b)$$

where [DNA] is the concentration of CT-DNA in base pairs, the apparent absorption coefficients ε_a, ε_f and ε_b correspond to A_{obsed}/[Ru], the absorbance for the free ruthenium complex, and the absorbance for the ruthenium complex in fully bound form, respectively. K is the equilibrium binding constant, C_t is the total metal complex concentration in nucleotides and s is the binding site size.

Viscosity measurements were carried out using an Ubbelodhe viscometer maintained at a constant temperature at 25.0 (±0.1) °C in a thermostatic bath. DNA samples approximately 200 base pairs in average length were prepared by sonicating in order to minimize complexities arising from DNA flexibility [27]. Flow time was measured with a digital stopwatch, and each sample was measured three times, and an average flow time was calculated. Relative viscosities for DNA in the presence and absence of complexes were calculated from the relation $\eta=(t-t^0)/t^0$, where t is the observed flow time of the DNA-containing solution and t^0 is the flow time of buffer alone [13,28]. Data were presented as $(\eta/\eta_0)^{1/3}$ versus binding ratio [29], where η is the viscosity of DNA in the presence of complexes and η_0 is the viscosity of DNA alone.

Thermal denaturation studies were carried out with a Perkin–Elmer Lambda 35 spectrophotometer equipped with a Peltier temperature-controlling programmer (±0.1 °C). The melting temperature (T_m) was taken as the mid-point of the hyperchromic transition. The melting curves were obtained by measuring the absorbance at 260 nm for solutions of CT-DNA (80 μM) in the absence and presence of the Ru(II) complex (30 μM) as a function of the temperature. The temperature was scanned from 50 to 90 °C at a speed of 1 °C min^{-1}.

For the gel electrophoresis experiment, supercoiled pBR 322 DNA (0.1 μg) was treated with the Ru(II) complexes in buffer B, and the solution was then irradiated at room temperature with a UV lamp (365 nm, 10 W). The samples were analyzed by electrophoresis for 1.5 h at 80 V on a 0.8% agarose gel in TBE (89 mM Tris-borate acid, 2 mM EDTA, pH = 8.3). The gel was stained with 1 μg/ml ethidium bromide and photographed on an Alpha Innotech IS–5500 fluorescence chemiluminescence and visible imaging system.

4.4. Cytotoxicity assay in vitro

Standard 3-(4,5-dimethylthiazole)-2,5-diphenyltetraazolium bromide (MTT) assay procedures were used [30]. Cells were placed in 96-well microassay culture plates (8×10^3 cells per well) and grown overnight at 37 °C in a 5% CO_2 incubator. Compounds tested were then added to the wells to achieve final concentrations ranging from 10^{-6} to 10^{-4} M. Control wells were prepared by addition of culture medium (100 μL). The culture medium and cisplatin were used as negative and positive control, respectively. The plates were incubated at 37 °C in a 5% CO_2 incubator for 48 h. Upon completion of the incubation, stock MTT dye solution (20 μL, 5 mg mL^{-1}) was added to each well. After 4 h incubation, buffer (100 μL) containing N,N-dimethylformamide (50%) and sodium dodecyl sulfate (20%) was added to solubilize the MTT formazan. The optical density of each well was then measured on a microplate spectrophotometer at a wavelength of 490 nm. The IC_{50} values were determined by plotting the percentage viability versus

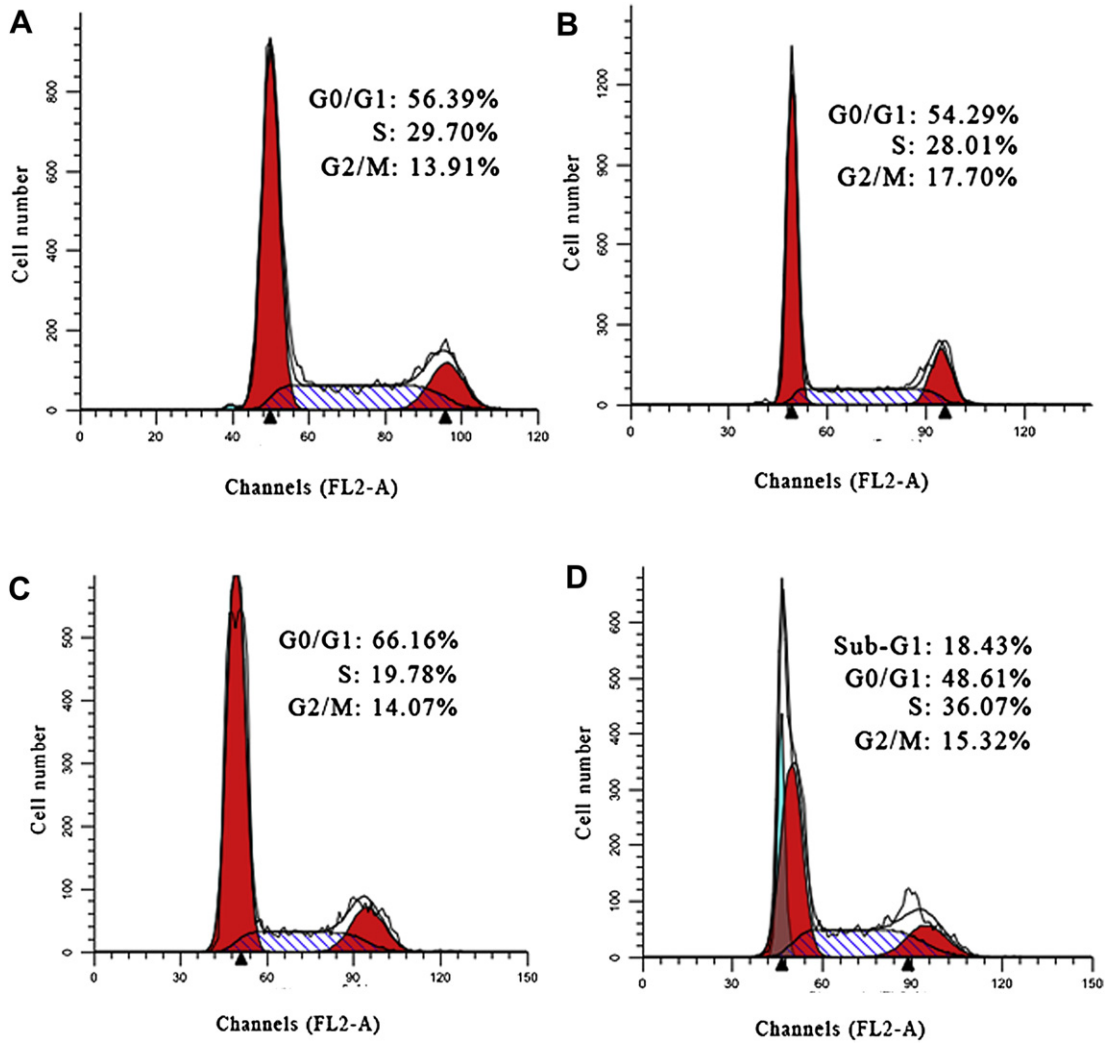

Fig. 9. Cell cycle status of the BEL-7402 and HepG-2 cells after treatment with complex **1** (25 μM) for 24 h. A (untreatment of BEL-7402), B (complex 1 + BEL-7402), C (untreatment of HepG-2) and D (complex 1 + HepG-2).

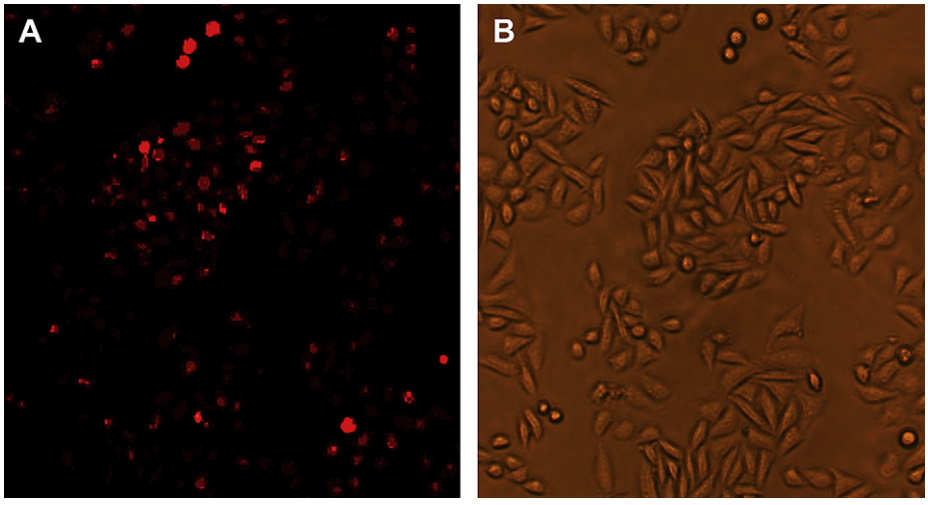

Fig. 10. BEL-7402 cells incubated with complex **2** (50 μM) for 48 h. A imaged by fluorescence microscopy. B imaged under fluorescence and visible light. Note that the cytoplasm is stained with the Ru(II) complex.

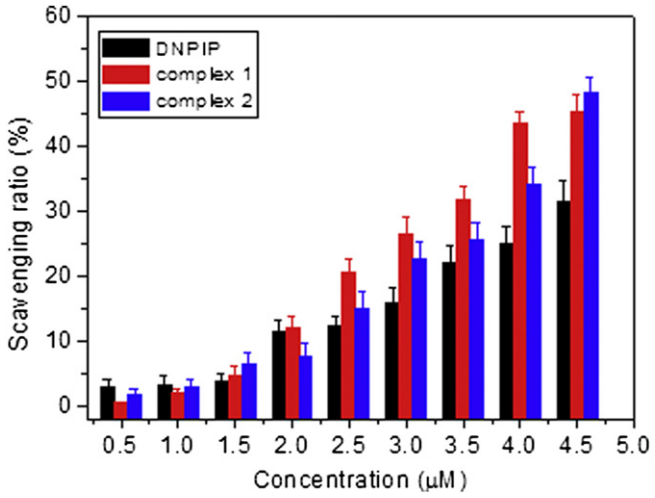

Fig. 11. Scavenging effect of the ligand DNPIP and complexes **1** and **2** on hydroxyl radicals. Experiments were performed in triplicate.

concentration on a logarithmic graph and reading off the concentration at which 50% of cells remain viable relative to the control. Each experiment was repeated at least three times to get the mean values. Three different tumor cell lines were the subjects of this study: BEL-7402, HepG-2 and MCF-7.

4.5. Apoptosis assessment by AO/EB staining

Apoptosis studies were performed with a staining method utilizing acridine orange (AO) and ethidium bromide (EB) [31]. According to the difference in membrane integrity between necrotic and apoptosis. AO can pass through cell membrane, but EB cannot. Under fluorescence microscope, living cells appear green. Necrotic cells stain red but have a nuclear morphology resembling that of viable cells. Apoptosis cells appear green, and morphological changes such as cell blebbing and formation of apoptotic bodies will be observed.

A monolayer of BEL-7402 cells was incubated in the absence and presence of complex **2** at concentration of 25 μM at 37 °C and 5% CO_2 for 48 h. Then each cell culture was stained with AO/EB solution (100 μg ml^{-1} AO, 100 μg ml^{-1} EB). Samples were observed under a fluorescence microscope.

4.6. Flow cytometric analysis

BEL-7402 cells were seeded into six-well plates (Costar, Corning Corp., New York) at a density of 2×10^5 cells per well and incubated for 24 h. The cells were cultured in RPMI 1640 supplemented with 10% FBS and incubated at 37 °C and 5% CO_2. The medium was removed and replaced with medium (final DMSO concentration, 1% v/v) containing complex **1** (25 μM). After incubation for 24 h or 48 h, the cell layer was trypsinized and washed with cold PBS (phosphate buffered saline) and fixed with 70% ethanol. 20 mL of RNAse (0.2 mg/ml) and 20 mL of propidium iodide (0.02 mg/ml) were added to the cell suspensions and incubated at 37 °C for 30 min. Then the samples were analyzed by a FACS Calibur flow cytometer (Becton Dickinson & Co., Franklin Lakes, NJ). The number of cells analyzed for each sample was 10,000 [32].

Table 2
The scavenging ratios (%) of ligand and complexes against ˙OH.

Comp	Average inhibition (%) for ˙OH								
	0.5	1.0	1.5	2.0	2.5	3.0	3.5	4.0	4.5 (μM)
DNPIP	3.08	3.34	3.86	11.57	12.34	15.94	22.11	24.94	31.61
1	0.51	2.06	4.88	12.08	20.57	26.48	31.88	43.44	45.24
2	1.80	3.08	6.43	7.71	15.17	22.62	25.71	34.19	48.33

4.7. Celluar uptake study

Cells were placed in 24-well microassay culture plates (4×10^4 cells per well) and grown overnight at 37 °C in a 5% CO_2 incubator. Compounds tested (50 μM) were then added to the wells. The plates were incubated at 37 °C in a 5% CO_2 incubator for 24 h. Upon completion of the incubation, the wells were washed three times with PBS, after removing the culture medium, the cells were visualized under fluorescent microscopy.

4.8. Scavenger measurements of hydroxyl radical (˙OH)

The hydroxyl radical (˙OH) in aqueous media was generated by the Fenton system [18]. The solution of the tested complexes was prepared with DMF (N,N-dimethylformamide). The 5 ml of assay mixture contained following reagents: safranin (28.5 μM), EDTA-Fe(II) (100 μM), H_2O_2 (44.0 μM), the tested compounds (0.5–4.5 μM) and a phosphate buffer (67 mM, pH = 7.4). The assay mixtures were incubated at 37 °C for 30 min in a water bath. Then the absorbance was measured at 520 nm. All the tests were run in triplicate and expressed as the mean. A_i was the absorbance in the presence of the tested compound; A_0 was the absorbance in the absence of tested compounds; A_c was the absorbance in the absence of tested compound, EDTA-Fe(II), H_2O_2. The suppression ratio (η_a) was calculated on the basis of $(A_i - A_0)/(A_c - A_0) \times 100\%$.

Acknowledgments

This work was supported by the National Nature Science Foundation of China (No. 30800227, 31070858) and Guangdong Pharmaceutical University for financial supports.

References

[1] C.X. Zhang, S. Lippards, Chem. Biol. 7 (2003) 481–489.
[2] E. Wong, C.M. Giandomenico, Chem. Rev. 99 (1999) 2451–2466.
[3] B. Rosenberg, L. VanCamp, T. Kriagas, Nature 205 (1965) 698–699.
[4] B. Rosenberg, L. VanCamp, J.E. Trosko, V.H. Mansour, Nature 222 (1969) 385–387.
[5] I. Bratsos, S. Jedner, T. Gianferrara, E. Alessio, Chimia 61 (2007) 692–697.
[6] X. Meng, M.L. Leyva, M. Jenny, I. Gross, S. Benosman, B. Harlepp, P. Hébraud, A. Boos, P. Wlosik, P. Bischoff, C. Sirlin, M. Pfeffer, J.P. Loeffler, C. Gaiddon, Cancer Res. 69 (2009) 5458–5466.
[7] T.F. Chen, Y.N. Liu, W.J. Zhen, J. Liu, Y.S. Wong, Inorg. Chem. 49 (2010) 6366–6368.
[8] U. Schatzschneider, J. Niesel, I. Ott, R. Gust, H. Alborzinia, S. Wölfl, ChemMedChem. 3 (2008) 1104–1109.
[9] Y.J. Liu, C.H. Zeng, H.L. Huang, L.X. He, F.H. Wu, Eur. J. Med. Chem. 45 (2010) 564–571.
[10] J.G. Liu, B.H. Ye, H. Li, Q.X. Zhen, L.N. Ji, Y.H. Fu, J. Inorg. Biochem 76 (1999) 265–271.
[11] S. Shi, J. Liu, L. Li, K.C. Zheng, C.P. Tan, L.M. Chen, L.N. Ji, Dalton Trans. (2005) 2038–2046.
[12] D.L. Arockiasamy, S. Radhika, R. Parthasarathi, B.U. Nair, Eur. J. Med. Chem. 44 (2009) 2044–2051.
[13] S. Satyanarayana, J.C. Dabrowiak, J.B. Chaires, Biochemistry 32 (1993) 2573–2584.
[14] Y.J. Liu, C.H. Zeng, Z.H. Liang, J.H. Yao, H.L. Huang, Z.Z. Li, F.H. Wu, Eur. J. Med. Chem. 45 (2010) 3087–3095.
[15] V. Rajendiran, M. Murali, E. Suresh, S. Sinha, K. Somasundaram, M. Palaniandavar, Dalton Trans. (2008) 148–163.
[16] Y.J. Liu, Z.H. Liang, Z.Z. Li, C.H. Zeng, J.H. Yao, H.L. Huang, F.H. Wu, Biometals 23 (2010) 739–752.
[17] H.J. Yu, S.M. Huang, L.Y. Li, H.N. Jia, H. Chao, Z.W. Mao, J.Z. Liu, L.N. Ji, J. Inorg. Biochem 103 (2009) 881–890.
[18] J.A. Hickman, Cancer Metast Rev 11 (1992) 121–139.
[19] K. Tsai, T.G. Hsu, K.M. Hsu, H. Cheng, T.Y. Liu, C.F. Hsu, C.W. Kong, Free Radical. Biol. Med. 31 (2001) 1465–1472.

[20] N. Udilova, A.V. Kozlov, W. Bieberschulte, K. Frei, K. Ehrenberger, H. Nohl, Biochem. Pharm. 65 (2003) 59–65.
[21] H.L. Huang, Y.J. Liu, C.H. Zeng, L.X. He, F.H. Wu, Dna Cell Biol. 29 (2010) 261–270.
[22] J. Marmur, J. Mol. Biol 3 (1961) 208–218.
[23] M.E. Reichmann, S.A. Rice, C.A. Thomas, P. Doty, J. Am. Chem. Soc. 76 (1954) 3047–3053.
[24] M. Yamada, Y. Tanaka, Y. Yoshimoto, S. Kuroda, I. Shimao, Bull. Chem. Soc. Jpn. 65 (1992) 2007–2009.
[25] B.P. Sullivan, D.J. Salmon, T.J. Meyer, Inorg. Chem. 17 (1978) 3334–3341.
[26] M.T. Carter, M. Rodriguez, A. Bard, J. Am. Chem. Soc. 111 (1989) 8901–8911.
[27] J.B. Chaires, N. Dattagupta, D.M. Crothers, Biochemistry 21 (1982) 3933–3940.
[28] S. Satyanaryana, J.C. Dabrowial, J.B. Chaires, Biochemistry 31 (1992) 9319–9324.
[29] G. Cohen, H. Eisenberg, Biopolymers 8 (1969) 45–55.
[30] T. Mosmann, J. Immunol. Methods 65 (1983) 55–63.
[31] D.L. Spector, R.D. Goldman, L.A. Leinwand, In Cells: a Laboratory Manual, vol. 1, Cold Spring Harbor Laboratory Press, New York, 1998, (Chapter 15).
[32] K.K. Lo, T.K. Lee, J.S. Lau, W.L. Poon, S.H. Cheng, Inorg. Chem. 47 (2008) 200–208.